K. J. Bathe
Associate Professor.
Mem. ASME

C. A. Almeida
Graduate Student.

Department of Mechanical Engineering,
Massachusetts Institute
of Technology,
Cambridge, Mass. 02139

A Simple and Effective Pipe Elbow Element—Interaction Effects

Our elbow element presented in an earlier communication is enhanced to account for interaction effects between elbows and rigid flanges, elbows of different curvatures, and elbows joining straight pipe sections. The interaction effects are modeled by including the appropriate additional strain terms in the stiffness matrix formulation and by using a penalty procedure to enforce the continuity of the derivatives in the pipe skin radial displacements. The enhancement in the formulation has been implemented and the results of various sample analyses are presented.

1 Introduction

In a previous communication, we presented a basic elbow pipe element [1], which we formulated using the displacement-based finite element method. The essential ingredients of the formulation are the specific displacement assumptions used and the stress and strain components included in the evaluation of the strain energy of the element.

The displacements used to formulate the element are, first, axial, torsional, and bending displacements with the assumption that the cross section of the elbow remains plane. Considering the element in Fig. 1, we have the cubic displacement interpolation

$$u_i(r,s,t) = \sum_{k=1}^{4} h_k u_i^k + t\sum_{k=1}^{4} \bar{a}_k h_k V_{ti}^k + s\sum_{k=1}^{4} \bar{a}_k h_k V_{si}^k;\ i = 1,2,3 \tag{1}$$

with

$$\mathbf{V}_t^k = \theta^k \times {}^0\mathbf{V}_t^k$$
$$\mathbf{V}_s^k = \theta^k \times {}^0\mathbf{V}_s^k \tag{2}$$

where

- r,s,t = isoparametric coordinates [2]
- u_i = Cartesian displacement of material point (r,s,t)
- $h_k(r)$ = isoparametric interpolation functions [1,2]
- u_i^k = Cartesian displacements of nodal point k
- θ^k = rotations at nodal point k
- $\bar{a}_k$ = outer radius of element at nodal point k
- ${}^0V_{ti}^k$ = component i of unit vector ${}^0\mathbf{V}_t^k$, in direction t at nodal point k
- ${}^0V_{si}^k$ = component i of unit vector ${}^0\mathbf{V}_s^k$, in direction s at nodal point k

The displacement interpolations in equation (1) correspond to the displacements of a beam with a circular cross section which does not distort either in or out of its plane.

The second displacement assumption is that the elbow can ovalize with the displacement patterns, see Fig. 2,

$$w_\xi(r,\phi) = \sum_{k=1}^{4}\Bigg(\underbrace{\sum_{m=1}^{N_c} h_k c_m^k \sin 2m\phi}_{\text{in-plane bending}} + \underbrace{\sum_{m=1}^{N_d} h_k d_m^k \cos 2m\phi}_{\text{out-of-plane bending}}\Bigg) \tag{3}$$

where the assumption is that (see reference [1])

$$w_\zeta = -\frac{dw_\xi}{d\phi} \tag{4}$$

and the c_m^k and d_m^k, $k = 1, 2, 3, 4$, are the unknown generalized ovalization displacements. Depending on the pipe geometry and the type of loading, it can be sufficient to include only the first, or first two, terms of one (or both) double summation(s). In the implementation of the element, we have allowed N_c to be 0 (no ovalization), 1, 2, or 3, and similarly for N_d [1]. The total displacements of the element are the sum of the displacements presented in equations (1) and (3). Hence, for example, with N_c and N_d equal to 3, a typical nodal point k carries the unknown displacements

$$\mathbf{u}^{kT} = [u_1^k\ u_2^k\ u_3^k\ \theta_1^k\ \theta_2^k\ \theta_3^k \mid c_1^k\ c_2^k\ c_3^k \mid d_1^k\ d_2^k\ d_3^k] \tag{5}$$

The element stiffness matrix of the elbow was obtained by including in the strain energy the usual longitudinal and shear strains corresponding to a curved circular cross section beam whose cross section does not distort and the strains due to ovalization. Using the coordinate axes defined in Figs. 1 and 2, the ovalization strains included were

$$(\epsilon_{\eta\eta})_{ov} = \frac{w_R}{R - a\cos\phi} \tag{6}$$

and

$$(\epsilon_{\xi\xi})_{ov} = -\frac{1}{a^2}\left[w_\zeta + \frac{d^2 w_\zeta}{d\phi^2}\right]\zeta \tag{7}$$

Contributed by the Applied Mechanics Division for publication in the JOURNAL OF APPLIED MECHANICS.
Discussion on this paper should be addressed to the Editorial Department, ASME, United Engineering Center, 345 East 47th Street, New York, N.Y. 10017, and will be accepted until two months after final publication of the paper itself in the JOURNAL OF APPLIED MECHANICS. Manuscript received by ASME Applied Mechanics Division, March, 1981; final revision, July, 1981.

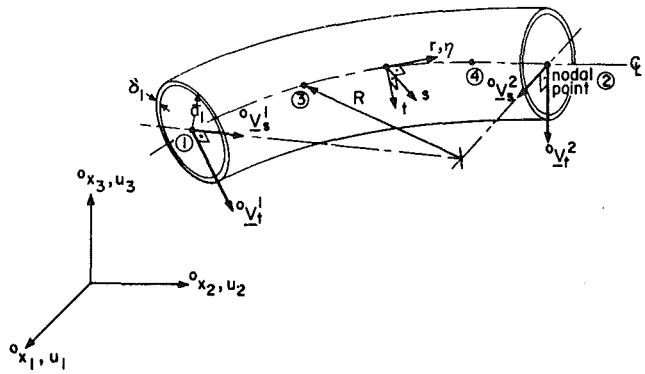

Fig. 1 Geometry of pipe elbow element

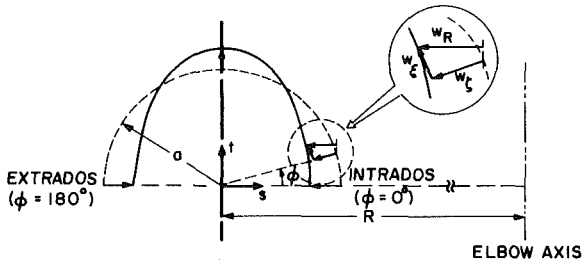

Fig. 2 Displacement of deformed cross section. (First von Kármán mode; w_ζ is shown negative.) Pipe mean radius is a.

The basic assumption in using the foregoing strain components only is that, in essence, each differential length of the elbow can ovalize independently, although by virtue of using equation (3), the ovalization displacements are continuous within an element and across element boundaries. Therefore, the interaction effects in the ovalization between elbows of different curvatures, an elbow and a straight pipe section, and an elbow and a rigid flange cannot be properly modeled. As we pointed out in [1], to render the element applicable to such situations, it is necessary to extend the basic formulation.

The objective in this paper is to amend our element formulation given in [1] in a very simple way to also account for interaction effects. This is achieved by including in the formulation additional important strain terms formulation that are identified using thin shell theory, and using a penalty procedure to enforce the required continuity conditions.

In the next section of this paper, we discuss the additional strain terms that are included in the formulation so that the element is applicable to the modeling of interaction effects. The presentation shows that it is then also necessary to enforce continuity in the derivatives of the ovalization displacements w_ζ with respect to the longitudinal membrane coordinate η. This continuity is imposed using a penalty procedure as discussed in Section 3. The amendments in the formulation of the element have been implemented in the computer program ADINAP, and in Section 4 we give the results obtained in the analyses of some problems.

2 Strain Terms Used in our Elbow Formulation

Considering the skin of the elbow to be a doubly curved thin shell [3], we can identify the following important strain terms, which have not been included in our original formulation and which are due to a variation of ovalization along the longitudinal axis of the elbow,

$$(\epsilon^I_{\eta\eta})_{ov} = -\left[\left(\frac{1}{R-a\cos\phi}\right)^2 \frac{d^2 w_\zeta}{d\theta^2}\right]\zeta \tag{8}$$

and

$$(\gamma^I_{\eta\xi})_{ov} = \left(\frac{1}{R-a\cos\phi}\right)\frac{dw_\xi}{d\theta} \tag{9}$$

In equations (8) and (9), the superscript "I" refers to the fact that these strain terms need be included in the formulation if interaction effects are important.

The strain term in equation (8) is due to longitudinal bending of the pipe skin and can directly be evaluated using the interpolation of w_ζ given in equations (3) and (4). However, since this term contains the second derivative of the pipe skin radial displacement, it is necessary to enforce in the finite element formulation continuity in the first derivative [2]. This is achieved using a penalty procedure as described in Section 3.

The shear strain term in equation (9) is a function of $dw_\xi/d\theta$ and therefore only requires continuity in w_ξ, which is already assured in the formulation.

Using the strain expressions in equations (8) and (9) and the displacement interpolation in equations (3) and (4), we can now directly amend the strain-displacement matrix given in reference [1]. Namely, to include the foregoing strain terms in our elbow formulation, we simply need to add to the matrices $\mathbf{B}^k_{ov1}$ and $\mathbf{B}^k_{ov3}$ defined in reference [1], and the following contributions, respectively,

$$\mathbf{B}^{Ik}_{ov1} = \frac{d}{dr}\begin{bmatrix} \frac{dh_k}{dr} & (a^I_1 & a^I_2 & a^I_3) \\ h_k & (b^I_1 & b^I_2 & b^I_3) \\ & 0 & 0 & 0 \end{bmatrix} \tag{10}$$

where,

$$a^I_l = \left[\frac{2}{(R_n - a\cos\phi)\theta_n}\right]^2 (m)\cos(m\phi)\zeta \tag{11}$$

$$b^I_l = \left[\frac{2}{(R_n - a\cos\phi)\theta_n}\right]\sin(m\phi) \tag{12}$$

$m = 2l$; $R_n\theta_n$ = length of elbow at center line

$$\mathbf{B}^{Ik}_{ov3} = \frac{d}{dr}\begin{bmatrix} \frac{dh_k}{dr} & (\tilde{a}^I_1 & \tilde{a}^I_2 & \tilde{a}^I_3) \\ h_k & (\tilde{b}^I_1 & \tilde{b}^I_2 & \tilde{b}^I_3) \\ & 0 & 0 & 0 \end{bmatrix} \tag{13}$$

where,

$$\tilde{a}^I_l = -\left[\frac{2}{(R_n - a\cos\phi)\theta_n}\right]^2 (m)\sin(m\phi)\zeta \tag{14}$$

$$\tilde{b}^I_l = \left[\frac{2}{(R_n - a\cos\phi)\theta_n}\right]\cos(m\phi) \tag{15}$$

The foregoing expressions are for a curved pipe. If a straight pipe is considered, the term $[2/(R_n - a\cos\phi)\theta_n]$ needs to be replaced by $[2/l]$ where l is the total length of the element.

3 Imposition of Continuity on Derivative of Pipe Skin Radial Displacement

The objective is to enforce continuity on the first derivative of the ovalization displacement w_ζ between elements without introducing additional degrees of freedom. In the classical analysis of beam structures, this continuity is achieved by introducing beam rotational degrees of freedom. However, we can enforce the continuity in our formulation without the use of rotational degrees of freedom using a penalty

procedure. The basic technique in this method is to add the constraint to be achieved in the solution, say,

$$\text{CONSTRAINT} = 0 \tag{16}$$

to the variational indicator of the problem in the following form,

$$\Pi = U - W + \frac{\alpha}{2}\int_0^{2\pi} (\text{CONSTRAINT})^2\, d\phi \tag{17}$$

where U and W are the total strain energy and total potential of the external loads, respectively, and α is the penalty parameter. The solution obtained using equation (17) with $\delta\Pi = 0$ will satisfy the condition in equation (16) to the required accuracy provided α is selected to be sufficiently large [2, 4–6].

Considering our elbow element, we want to be able to impose the constraints corresponding to two different conditions: first, the fixity condition when an element is clamped to a rigid flange and, second, the continuity condition when elements are joined.

3.1 Fixity Condition. When an element is fixed or clamped to a rigid flange, as shown schematically in Fig. 3(*a*), the boundary conditions are that at $x = 0$ there is no ovalization and $dw_\zeta/dx = 0$. Hence, we have, corresponding to equation (3)

$$c_m^i = d_m^i = 0 \quad (\text{all } m) \tag{18}$$

and

$$\left[\frac{2}{(R_n - a\cos\phi)\theta_n}\right]\frac{dw_\zeta}{dr}\bigg|_{r=-1} = 0 \tag{19}$$

where

$$\frac{dw_\zeta}{dr}\bigg|_{r=-1} = -\sum_{k=1}^{4}\left(\sum_{m=1}^{N_c} 2m\, c_m^k \frac{dh_k}{dr}\bigg|_{r=-1}\cos 2m\phi - \sum_{m=1}^{N_d} 2m\, d_m^k \frac{dh_k}{dr}\bigg|_{r=-1}\sin 2m\phi\right) \tag{20}$$

The constraint in equation (18) simply means that the ovalization degrees of freedom at node i must be set equal to zero, whereas the constraint in equation (19) is imposed with a penalty parameter. Using, in accordance with equation (16),

$$\text{CONSTRAINT} = \left[\frac{2}{(R_n - a\cos\phi)\theta_n}\frac{dw_\zeta}{dr}\bigg|_{r=-1} - 0\right] \tag{21}$$

then substituting into equation (17) and invoking the stationarity condition on Π results into the following penalty matrix

$$\mathbf{K}_p^F = \alpha\int_0^{2\pi} \mathbf{G}_F{}^T\left[\frac{2}{(R_n - a\cos\phi)\theta_n}\right]^2 \mathbf{G}_F\, d\phi \tag{22}$$

where

$$\mathbf{G}_F = [\ldots \bar{a}_1^k\ \bar{a}_2^k\ \bar{a}_3^k\ \bar{b}_1^k\ \bar{b}_2^k\ \bar{b}_3^k \ldots] \tag{23}$$

$$\bar{a}_m^k = -2m\frac{dh_k}{dr}\bigg|_{r=-1}\cos 2m\phi \tag{24}$$

$$\bar{b}_m^k = 2m\frac{dh_k}{dr}\bigg|_{r=-1}\sin 2m\phi \tag{25}$$

and $\mathbf{K}_p^F$ is defined corresponding to the degrees of freedom

$$\mathbf{u}^{F^T} = [\ldots \underbrace{c_1^k\ c_2^k\ c_3^k\ d_1^k\ d_2^k\ d_3^k}_{\text{node } k}\ \ldots] \tag{26}$$

The matrix $\mathbf{K}_p^F$ with a relatively large value of α is added using the usual direct stiffness matrix procedure [2] to enforce the constraint in equation (21). The study in Section 4 illustrates how an appropriate magnitude for α is chosen.

3.2 Continuity Condition. At the intersection of two elbow elements, as shown in Fig. 3(*b*), the ovalization is automatically continuous because the same ovalization degrees of freedom pertain to both elements. In addition, we have the continuity condition

$$\text{CONSTRAINT} = \left[\frac{2}{(R_n - a\cos\phi)\theta_n}\right]\frac{dw_\zeta}{dr}\bigg|_{r=+1} - \left[\frac{2}{(R_{n+1} - a\cos\phi)\theta_{n+1}}\right]\frac{dw_\zeta}{dr}\bigg|_{r=-1} \tag{27}$$

We impose this condition using the penalty method already employed in Section 3.1. Substituting into equation (17) from equation (27), we now obtain the penalty matrix

$$\mathbf{K}_p^C = \alpha\int_0^{2\pi} \mathbf{G}_C{}^T\,\mathbf{G}_C\, d\phi \tag{28}$$

where

$$\mathbf{G}_C = [\ldots \bar{a}_1^{k(n)}\ \bar{a}_2^{k(n)}\ \bar{a}_3^{k(n)}\ \bar{b}_1^{k(n)}\ \bar{b}_2^{k(n)}\ \bar{b}_3^{k(n)}\ \ldots \bar{a}_1\ \bar{a}_2\ \bar{a}_3\ \bar{b}_1\ \bar{b}_2\ \bar{b}_3 \ldots$$
$$\ldots \bar{a}_1^{k(n+1)}\ \bar{a}_2^{k(n+1)}\ \bar{a}_3^{k(n+1)}\ \bar{b}_1^{k(n+1)}\ \bar{b}_2^{k(n+1)}\ \bar{b}_3^{k(n+1)}\ \ldots] \tag{29}$$

$$\left.\begin{aligned} \bar{a}_m^{k(n)} &= -\left[\frac{2}{(R_n - a\cos\phi)\theta_n}\right]2m\frac{dh_k{}^{(n)}}{dr}\bigg|_{r=+1}\cos 2m\phi \\ \bar{b}_m^{k(n)} &= \left[\frac{2}{(R_n - a\cos\phi)\theta_n}\right]2m\frac{dh_k{}^{(n)}}{dr}\bigg|_{r=+1}\sin 2m\phi \end{aligned}\right\} k \neq 2 \tag{30, 31}$$

$$\left.\begin{aligned} \bar{a}_m^{k(n+1)} &= \left[\frac{2}{(R_{n+1} - a\cos\phi)\theta_{n+1}}\right]2m\frac{dh_k{}^{(n+1)}}{dr}\bigg|_{r=-1}\cos 2m\phi \\ \bar{b}_m^{k(n+1)} &= -\left[\frac{2}{(R_{n+1} - a\cos\phi)\theta_{n+1}}\right]2m\frac{dh_k{}^{(n+1)}}{dr}\bigg|_{r=-1}\sin 2m\phi \end{aligned}\right\} k \neq 1 \tag{32, 33}$$

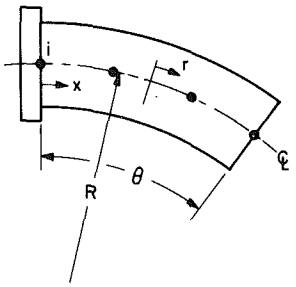

(a) ELBOW WITH A RIGID FLANGE AT NODE i

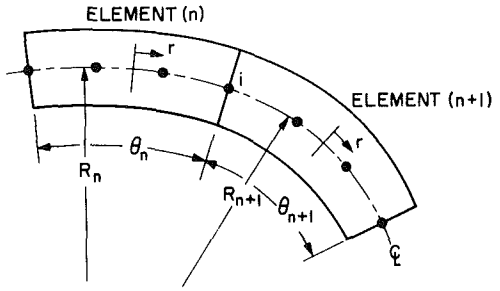

(b) ELBOWS OF DIFFERENT RADII JOINED AT NODE i

Fig. 3 Interactions considered in analyses

and for the common node (i) of the two elements,

$$\bar{a}_m = \left\{ -\left[\frac{2}{(R_n - a\cos\phi)\theta_n}\right]\frac{dh_2^{(n)}}{dr}\bigg|_{r=+1} + \left[\frac{2}{(R_{n+1} - a\cos\phi)\theta_{n+1}}\right]\frac{dh_1^{(n+1)}}{dr}\bigg|_{r=-1}\right\} 2m\cos 2m\phi \tag{34}$$

$$\bar{b}_m = \left\{ \left[\frac{2}{(R_n - a\cos\phi)\theta_n}\right]\frac{dh_2^{(n)}}{dr}\bigg|_{r=+1} - \left[\frac{2}{(R_{n+1} - a\cos\phi)\theta_{n+1}}\right]\frac{dh_1^{(n+1)}}{dr}\bigg|_{r=-1}\right\} 2m\sin 2m\phi \tag{35}$$

This penalty matrix corresponds to the degrees of freedom

$$\mathbf{u}^{cT} = [\ldots \underbrace{c_1^{k(n)}\ c_2^{k(n)}\ c_3^{k(n)}\ d_1^{k(n)}\ d_2^{k(n)}\ d_3^{k(n)}}_{\text{node } k \text{ of element } (n),\ k\neq 2} \ldots \underbrace{c_1\ c_2\ c_3\ d_1\ d_2\ d_3}_{\text{node } i} \ldots$$

$$\ldots \underbrace{c_1^{k(n+1)}\ c_2^{k(n+1)}\ c_3^{k(n+1)}\ d_1^{k(n+1)}\ d_2^{k(n+1)}\ d_3^{k(n+1)}}_{\text{node } k \text{ of element } (n+1),\ k\neq 1} \ldots] \tag{36}$$

4 Sample Analyses

We have implemented the foregoing enhancements to our elbow formulation in the computer program ADINAP [7]. The following analysis results are presented to indicate the applicability and effectiveness of these enhancements.

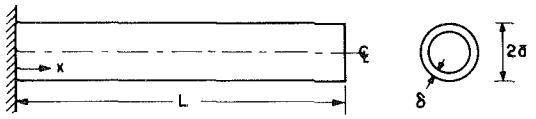

OVALIZATION BOUNDARY CONDITIONS

AT $x = 0$: $w_\zeta = 0.$, $\frac{dw_\zeta}{dx} = 0.$

AT $x = L$: $C_1 = 0.5$ in. (CORRESPONDING TO UNIT OVALIZATION IN FIRST VON KÁRMÁN MODE)

ANALYSIS PARAMETERS

$L = 4.8$ in. $\quad E = 2.8 \times 10^7$ psi

$\bar{\delta} = 8.0$ in.

$\delta = 0.37$ in.

Fig. 4 Straight cantilever pipe test problem, E = Young's modulus

4.1 Analysis of a Straight Pipe. The straight cantilever pipe shown in Fig. 4 was analyzed for a prescribed ovalization at its right end. The purpose of this analysis was to investigate the effects of the element size and penalty parameter size on the response predicted, and thus arrive at some guidelines for the use of the element in modeling more complex piping systems.

Figure 5 shows the response predicted in the analysis when using four equal size elements. It is seen that, although dw_ζ/dx is continuous, the second derivative of w_ζ with respect to x is strongly discontinuous at the junction of the first and second elements. Hence, the bending strain (in equation (8)) displays a large jump at this point and a finer finite element mesh is required at the fixed end if the stress distribution is to be predicted accurately.

The appropriate element size for stress continuity between elements is evaluated by recognizing that in the stiffness matrix the bending strain contribution due to equation (8) should be at least as large as the shearing strain contribution in equation (9). This condition gives that for an element in which the terms in equations (8) and (9) are important, we want $\delta/l > 1/4$ where l is the element length. Figure 6 shows the response predicted using a fine finite element idealization for which this criterion is satisfied. It is seen that in the predicted response, the second derivative of w_ζ is now continuous. It is also impoprtant to note that the ovalization displacement w_ζ has changed very little from the response given in Fig. 5.

To investigate the effect of the size of the penalty parameter α, the 16-element model of the cantilevered pipe was analyzed using the values of α listed in Fig. 7. As expected, when α is very small, the fixity condition at $x = 0$ is not properly imposed and when α is very large, the complete element stiffness matrix is singular. However, for a large range of α (see Cases 2 and 3) an identical response is predicted. In practice, it is effective to choose α equal to the largest value in the stiffness matrix corresponding to the ovalization degrees of freedom and this is done automatically in the program.

4.2 Analysis of a Flanged Pipe Bend. The flanged pipe bend shown in Fig. 8 was analyzed using the finite element model given. Figures 9–13 show the computed response for

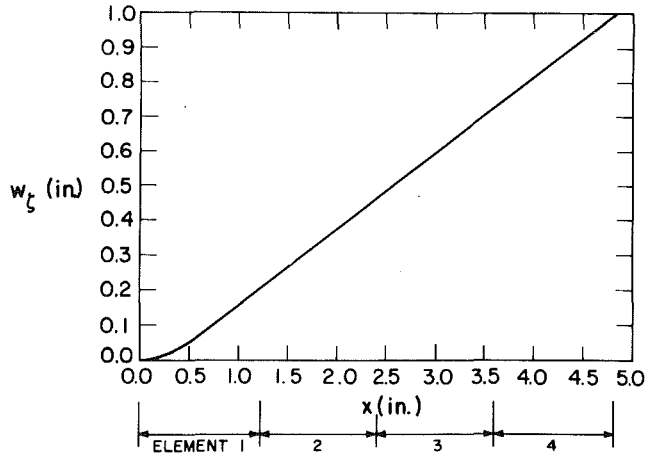

Fig. 5 Predicted response of cantilevered pipe using four equal elements

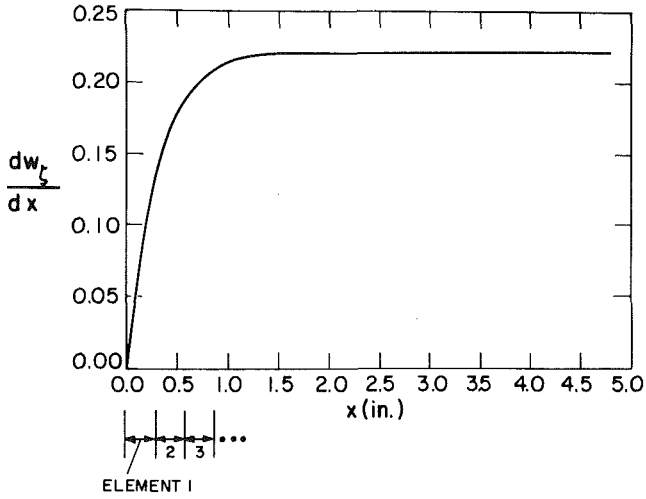

Fig. 6 (cont.)

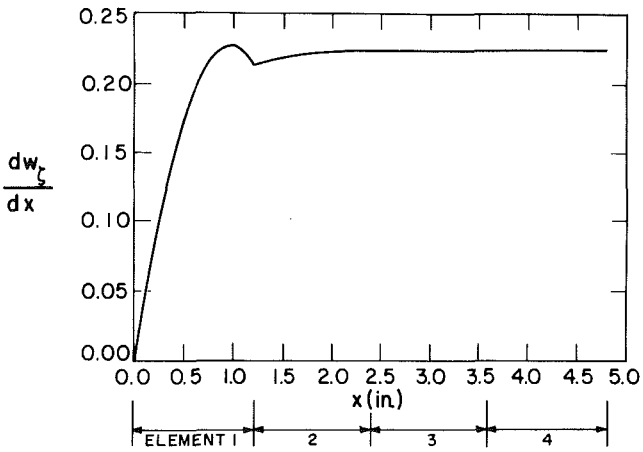

Fig. 5 (cont.)

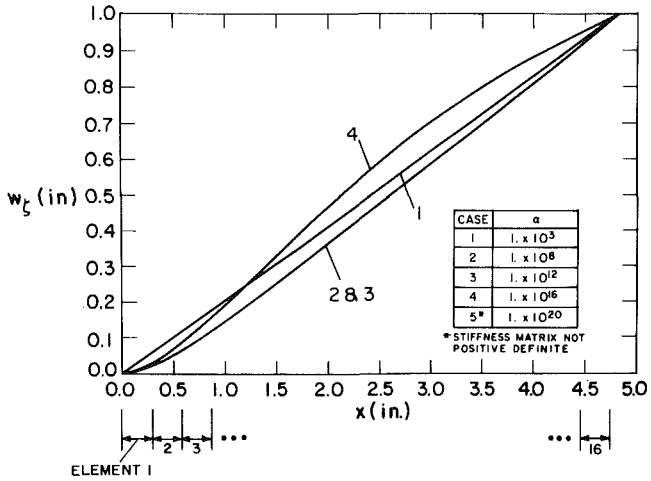

Fig. 7 Effect of size of penalty parameter on predicted response of cantilevered pipe

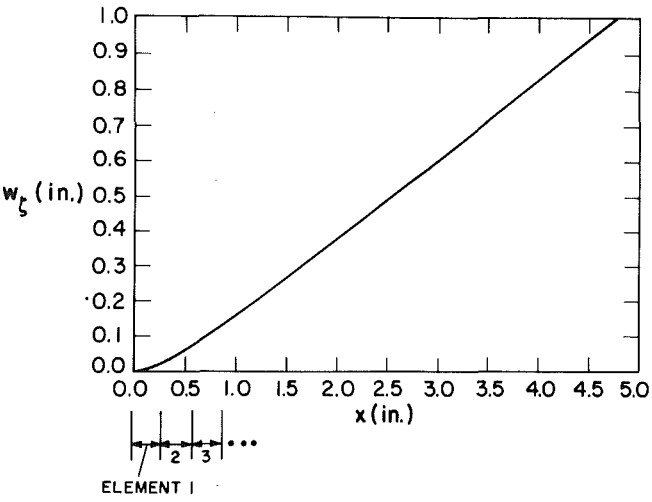

Fig. 6 Predicted response of cantilevered pipe using fine finite element idealization (same response obtained using 16 elements of length 0.3 in. or 6 elements of 0.3 in. and 1 element of 3.0 in.)

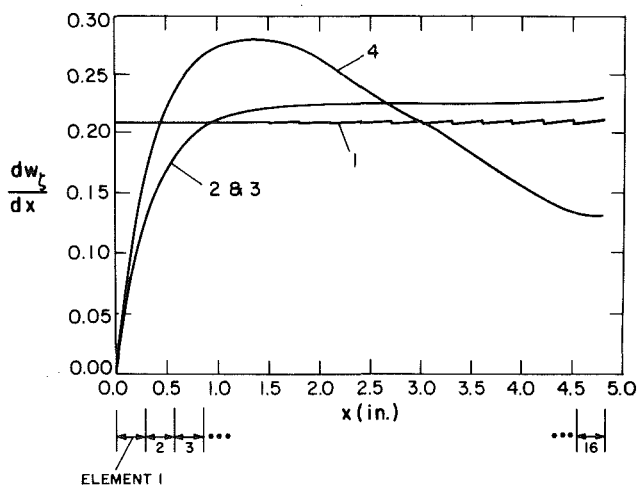

Fig. 7 (cont.)

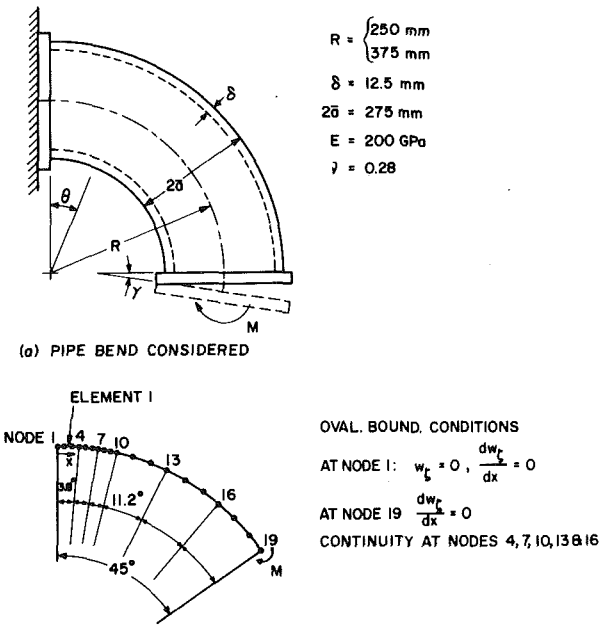

Fig. 8 Whatham pipe bend, E = Young's modulus, ν = Poisson's ratio

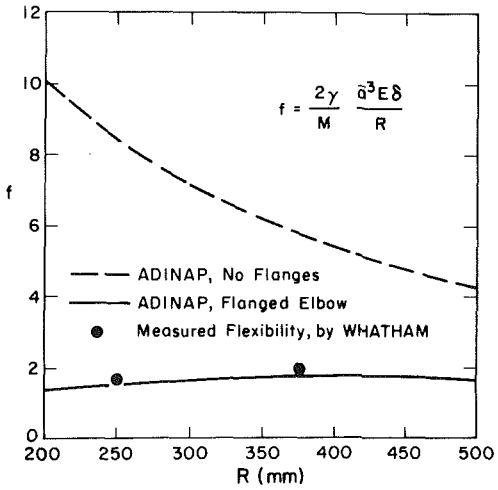

Fig. 9 Predicted flexibility factors for Whatham pipe bend

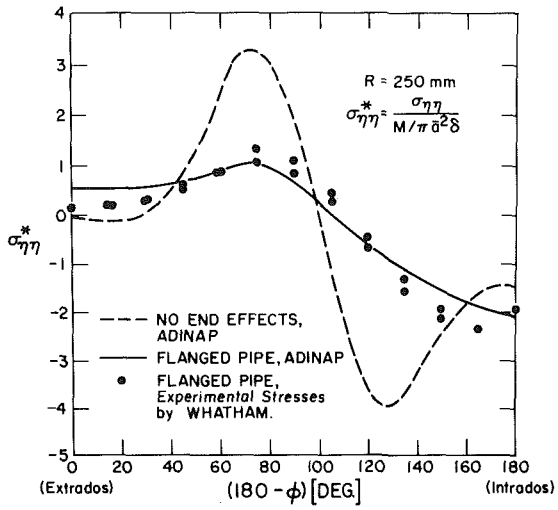

Fig. 10 Predicted longitudinal stresses at θ = 45 deg and at outside surface in analysis of Whatham pipe bend, R = 250 mm

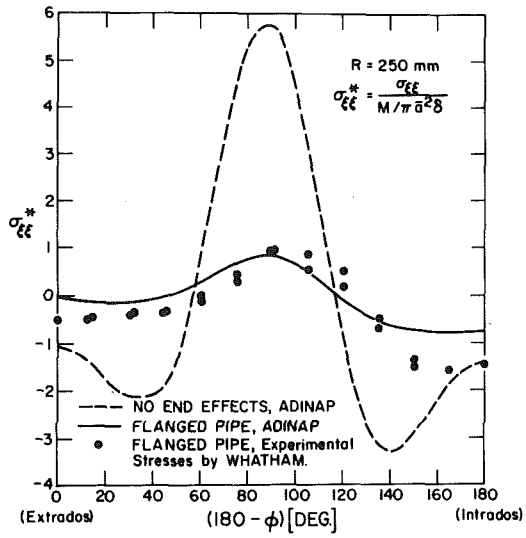

Fig. 11 Predicted circumferential stresses at θ = 45 deg and at outside surface in analysis of Whatham pipe bend, R = 250 mm

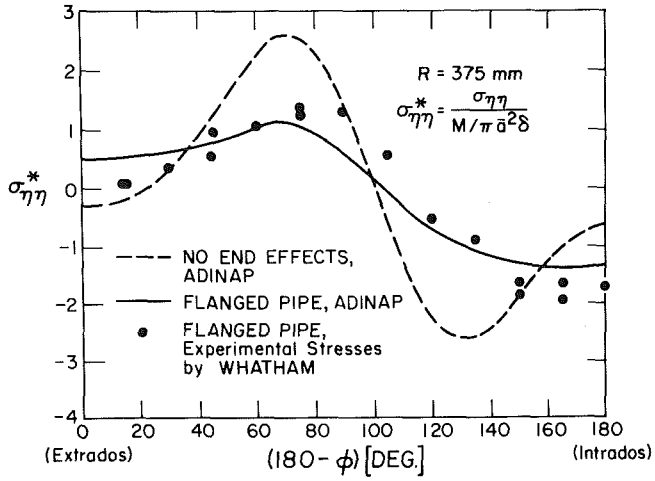

Fig. 12 Predicted longitudinal stresses at θ = 45 deg and at outside surface in analysis of Whatham pipe bend, R = 375 mm

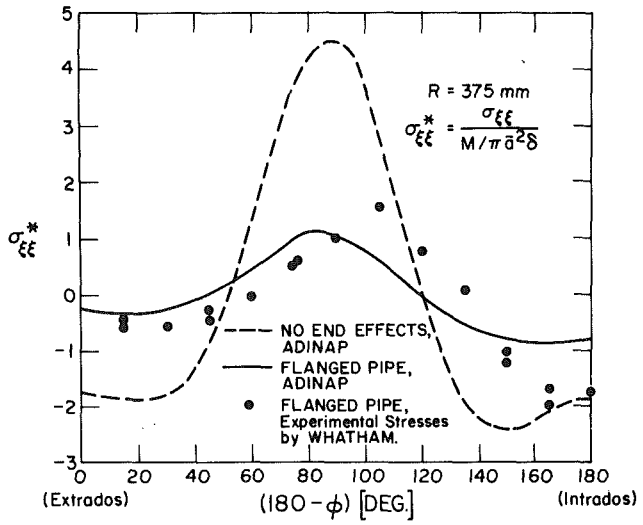

Fig. 13 Predicted circumferential stresses at θ = 45 deg and outside surface in analysis of Whatham pipe bend, R = 375 mm

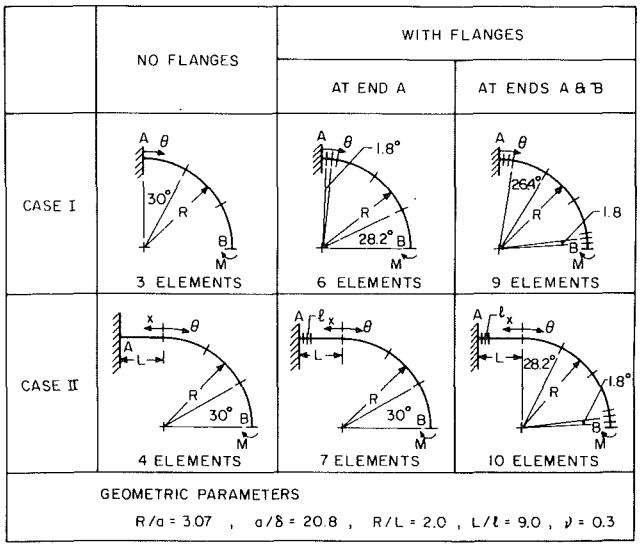

Fig. 14 Pipe bends and finite element models used

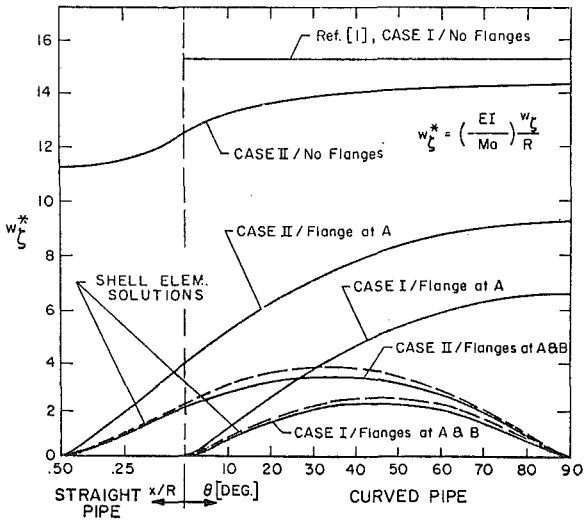

Fig. 15 Predicted ovalization response of bends defined in Fig. 14. Ovalization measured at $\phi = 90$ deg.

two different bend radii and give also experimental results [8]. It is seen that the correspondence between the computed and experimental flexibility factors and longitudinal stresses is good, but there is less good corrrespondence between the measured and computed circumferential stresses.

4.3 Analysis of a Second Pipe Bend. The pipe bend shown in Fig. 14 was analyzed in reference [1] and in previous studies [9, 10]. In these analyses, interaction effects were not considered. Figure 15 shows the response predicted when now including interaction effects using the idealizations described in Fig. 14. For comparison, also the response predicted using a finite element shell idealization of the piping system with flanges at A and B is shown. The shell element used in these analyses is the triangular flat 18 degrees of the freedom element described in [11]. The following shell element mesh was used: 12 layers of elements around half the circumference (one layer being two triangles), 9 layers for the 90 deg bend, and 3 layers for the straight. Thus, a total of 216 and 288 shell elements were used to model Case I/flanges at A and B and Case II/flanges at A and B, respectively. Figure 15 shows that the ovalizations predicted using our elbow element are close to the ovalizations calculated with the shell element idealizations. Considering the response of the piping structures, we note that the ovalizations of the piping systems are reduced very significantly when the interaction effects are included.

Conclusions

Our elbow element presented in reference [1] has been enhanced to also account for interaction effects with rigid flanges and straight piping sections. The interaction effects are included in a novel, but very simple and efficient manner using a penalty function formulation. The results of some sample solutions have been presented which indicate the applicability of the element. However, the total element formulation is based on a number of assumptions and further detailed studies of the element performance are required in order to identify the limit of range of problems for which the element can be employed.

Acknowledgment

We gratefully acknowledge the support of CNEN and PUC/RJ, Brazil, for C. A. Almeida's studies.

References

1 Bathe, K. J., and Almeida, C. A., "A Simple and Effective Pipe Elbow Element — Linear Analysis," ASME JOURNAL OF APPLIED MECHANICS, Vol. 47, No. 1, 1980, pp. 93–100.

2 Bathe, K. J., *Finite Element Procedures in Engineering Analysis,* Prentice-Hall, 1981.

3 Novozhilov, V. V., *Thin Shell Theory,* translated by P. G. Lowe, P. Noordhoff Ltd., Groningen, Netherlands, 1964.

4 Zienkiewicz, O. C., *The Finite Element Method,* McGraw-Hill, New York, 1977.

5 Felippa, C. A., "Interactive Procedures for Improving Penalty Function Solutions of Algebraic Systems," *International Journal of Numerical Methods in Engineering,* Vol. 12, 1978, pp. 821–836.

6 Oden, J. T., "Exterior Penalty Methods for Contact Problems in Elasticity," *Nonlinear Finite Element Analysis in Structural Mechanics* W. Wunderlich, et al., eds., S pringer-Verlag, Berlin, 1981.

7 ADINAP, Arthur D. Little Report, 1979.

8 Whatham, J. F., "In-Plane Bending of Flanged Elbows," *Proceedings, Metal Structures Conference,* the Institution of Engineers, Australia, Perth, Nov. 30–Dec. 1, 1978.

9 Clark, R. A., and Reissner, E., "Bending of Curved Tubes," *Advances in Applied Mechanics,* Vol. 2, 1951, pp. 93–122.

10 Sobel, L. H., "In-Plane Bending of Elbows," *Journal Computers and Structures,* Vol. 7, 1977, pp. 701–715.

11 Bathe, K. J., and Ho, L. W., "A Simple and Effective Element for Analysis of General Shell Structures," *Journal of Computers and Structures,* Vol. 13, 1981, pp. 673–681.